# Influence of the variability of soil profile properties on weak and strong seismic response

Stefania Gobbi, Luca Lenti, Maria Paola Santisi D'avila, Jean-François Semblat, Philippe Reiffsteck

# Influence of the variability of soil profile properties on weak and strong seismic response

Stefania Gobbi[a,*], Luca Lenti[a,d], Maria Paola Santisi d'Avila[b], Jean-François Semblat[c], Philippe Reiffsteck[a]

[a] Université Gustave Eiffel, IFSTTAR (GERS/SRO), Marne la Vallée, France

[b] Polytech'Lab, EA UNS 7498, Université Côte d'Azur, Sophia Antipolis, France

[c] IMSIA (UMR9219), CNRS, EDF, CEA, ENSTA Paris, Institut Polytechnique de Paris, France

[c] Cerema, Equipe-Projet MOUVGS, Sophia Antipolis, France

Corresponding author:

Stefania Gobbi

Université Gustave Eiffel, IFSTTAR (GERS/SRO)

14-20 Boulevard Newton - 77420 Champs sur Marne - France

Email: stefania.gobbi@ifsttar.fr

## ABSTRACT

Characterizing the potential effect of local site conditions on the amplification of ground motions is a critical aspect of seismic hazard and risk assessment. The aim of this study is to investigate the reliability and the limit of using the average shear wave velocity in the upper $30\,\mathrm{m}$ of the soil profile $v_{s,30}$, as single proxy, to characterize seismic site effects for weak and strong events.

To this regard, a dataset of 300 one-dimensional soil profiles with a given $v_{s,30}$ are generated through a Monte Carlo approach. Their seismic responses are computed for a set of 40 real accelerograms, with different seismic features. The vertical propagation from the bottom of the generated columns is modeled using a finite element spatial discretization, accounting for both linear and nonlinear soil behavior.

The site dominant frequency $f_0$ and the shear wave velocity gradient in the profile $B_{30}$ are proposed as proxies to characterize seismic site effects and the variability of the response spectra for the numerical signals, at the free surface of the set of columns, is discussed. Correlations between site-specific amplification factors deduced using the numerical response spectra and the proposed site proxies are analyzed for different sub-ranges of periods. The obtained amplification factors are then compared to those proposed by different international and national design codes.

The results, obtained under assumption of linear and nonlinear behavior of soil, emphasize the need to introduce complementary site parameters proxies, in addition to $v_{s,30}$, to characterize the expected site effects in design response spectra.



**Keywords:** Geotechnical properties, site effects, variability, average shear wave velocity, impedance contrast, response spectrum, Eurocode 8.

## 1. Introduction

Recent and past earthquakes, such as 1985 Mexico City, 1989 Loma Prieta, 1994 Northridge, 1995 Kobe events, among others, underline the need to characterize the effect of the local soil conditions on seismic site response prediction. It has been widely recognized that the seismic site effects are generally related to the stratigraphy, the surface topography, the impedance contrast and the rheology of the soils involved during the propagation of seismic waves [1].

Current seismic design codes consider the seismic site effects through a ground type classification solely based on the average shear velocity in the upper $30\,\mathrm{m}$ of the soil profile $v_{s,30}$ proposed by Borcherdt [2], neglecting the depth of the bedrock and the property of the soil below 30m. Nevertheless, it has been recognized that $v_{s,30}$ is a useful parameter to capture some features of the local site amplification effects [3–7].

However, several researches [8–15] show that $v_{s,30}$ cannot be used as the single-site proxy to discriminate soils in terms of seismic amplification over the whole frequency range of interest. To this regard, Steidl [16] and Park and Hashash [8] recommended the introduction of a depth-to-bedrock parameter since they found that the previsions based on $v_{s,30}$ are over and under conservative for deep sediments at short and long periods, respectively. Many alternatives to $v_{s,30}$ are proposed to improve site soil characterization accounting for additional information on the shear wave velocity profile with depth, the site dominant frequency $f_0$, the impedance contrast between sediments and bedrock and the depth to the bedrock.

Various studies [11,12,17–21] propose new site classification based on a combination of these different proxies. Gallipoli and Mucciarelli [21] and Cadet et al. [11] propose a two-parameters site classification approach through the dominant frequency $f_0$ and the average

shear wave velocity $v_s(\bar{z})$ in the shallow soil up to the reference depth $\bar{z}$. Kotha et al. [17] introduce a new approach classification characterized by the kernel density distributions of $v_{s,30}$, $v_{s,10}$, $H_{800}$ and the predominant period.

Recently, several researchers explore the performance of different site proxies in order to reduce the aleatory variability on the seismic prediction. Derras et al. [14] investigate the performance of four site condition proxies, $v_{s,30}$, $f_0$, the topographical slope and the depth $H_{800}$ (the depth where the shear wave velocity $v_s$ reaches $800\,\mathrm{m/s}$) using a neural networks approach, in order to assess their benefits to reduce the uncertainty of the site response. They conclude that the best single-proxy is $v_{s,30}$ for periods below 0.6 s and $f_0$ or $H_{800}$ at longer periods and that the best pair is ($v_{s,30}, H_{800}$) at short periods and ($f_0, H_{800}$) at long periods. Stambouli et al. [22] conduct a numerical investigation on 858 soil columns corresponding to real sites profiles from Japan, USA, and Europe. They show that the best performing site proxy is the impedance contrast between bedrock velocity and minimum surface velocity but even the pair ($v_{s,30}, f_0$) can reduce significantly the variability of the site response at least around 60%.

Lately, Chuanbin et al. [23] study the best performing site proxies for the linear characterization of the site response using 1840 ground-motion recordings from a KiK-net database. They focus their study on the dominant period of the site $T_0$, the site depths $Z_{0.8}$ and $Z_{1.0}$, which are measured site depths to layers having shear-wave velocity 0.8 and 1.0 km/s, respectively. They demonstrate that predictions based on the configuration using $T_0$ as the primary and $v_{s,30}$ as the secondary proxy can induce a significant reduction in site-to-site amplification variability.

Ciancimino et al. [24] adopt some classical proxies for site characterization in the context of

seismic site effect estimation. Their reliability is evaluated, under the assumption of linear regime, and compared to the ground type classification adopted in the Eurocode 8 [25], New Zealand Standard [26] and that suggested by Pitilakis et al. [18].

Following these recent reviews, the prediction of the seismic site response using only a single proxy over the whole period range does not seem satisfactory. Hence, to improve the site amplification estimation, it is advisable to use a combination of site proxies rather than a single site proxy. Based on this idea, the goal of the present research is to assess the correlation with the site amplification of some site parameters used to characterize the site condition, with the aim of improving the expected ground motion prediction.

In this research, the site dominant frequency $f_0$ and the shear wave velocity gradient $B_{30}$ are selected as complementary proxies, in addition to $v_{s,30}$, and applied to a wide variety of soil profiles with given $v_{s,30}$ and $H_{800}$. The two proposed proxies has been selected because they can be estimated, without excessive cost, by geophysical methods applied to ambient vibrations or seismic motions, recorded using temporary instruments located at the soil surface [27].

Then, since the nonlinear behavior of soils has been recognized as an important factor in site response [28,29], the second aim of this work is to explore how these site parameter proxies allow to capture and account for the nonlinear component of site response.

## 2. Methodology

The stratigraphy of a set of soil profiles with a given average shear wave velocity in the upper $30\,\mathrm{m}$ $v_{s,30}$ is randomly generated, according to the Monte Carlo method. Consequently, all the generated profiles belong to the same ground type in the Eurocode classification [25].

The seismic wavefield along these soil profiles has been computed using the finite element method (FEM) for spatial discretization and the Newmark algorithm for time discretization,

implemented in the SWAP_3C FEM package [30,31]. The highest-amplitude horizontal component of a wide variety of recorded earthquakes, representative of regions of low to moderate intensity, is applied as input motion at the base of each soil profile. These recorded signals are propagated along each soil profile and the ground response at the surface is evaluated in both cases of linear and nonlinear soil behavior.

Results are presented with regard to the amplification factors adopted by Ciancimino et al. [24], in different period ranges, in order to distinguish short-, mid- and long-period amplification factors. Differences between the response spectra of numerical signals at the soil surface and the reference spectrum proposed by European buildings codes [25] are then quantified and discussed.

### 2.1 Set of generated soil profiles for the statistical analysis

The parameters chosen for the set of soil profiles are the average shear wave velocity $v_{s,30} = 270\,\mathrm{m/s}$, corresponding to the ground type C according to the Eurocode 8 [25], the soil depth of $30\,\mathrm{m}$, the number of layers equal to 4 and the density $\rho = 1850\,\mathrm{kg/m^3}$. The geotechnical properties assumed for the bedrock are the density $\rho_b = 2200\,\mathrm{kg/m^3}$ and the shear wave velocity $v_{sb} = 1000\,\mathrm{m/s}$.

The properties of each layer are generated considering each stochastic parameter uniformly distributed in a given range. The soil layer thickness ranges in $[1-15\,\mathrm{m}]$, the shear wave velocity in $[100-800\,\mathrm{m/s}]$ and 4 soil types can be randomly targeted.

Each soil type from 1 to 4 is associated to a plasticity index $PI = 0, 5, 10$ and $20\%$, respectively. Yokota et al. [32] have shown that normalized shear modulus reduction curve for different types of soils can be expressed by a set of formulas in the absence of available test data. To this regard, a normalized shear modulus reduction curve, as a function of the

shear strain $\gamma$, is derived using the four-parameter model proposed by Darendeli [33] to characterize normalized modulus reduction formulation:

$$G(\gamma)/G_0 = 1/\left[1+(\gamma/\gamma_r)^{\alpha}\right] \quad (1)$$

assuming a normal consolidated soil (over-consolidation ratio $OCR = 1$). The reference shear strain is defined as $\gamma_r = \left(\phi_1 + \phi_2\, PI \cdot OCR^{\phi_3}\right)\sigma'^{\phi_4}_{v0}$, where from $\phi_1$ to $\phi_4$ are parameters that relate the normalized modulus reduction curve to soil type and loading conditions estimated on the basis of statistical analysis ($\phi_1 = 0.0352$, $\phi_2 = 0.001$, $\phi_3 = 0.3246$, $\phi_4 = 0.3483$) and $\alpha = 0.92$.

The vertical effective stress $\sigma'_{v0}$ is calculated each 5 m using the chosen soil density $\rho = 1850\,\mathrm{kg/m^3}$, to account for the variation of the shear modulus decay curve with depth.

The normalized shear modulus reduction curves employed for the four soil types, associated to a different plasticity index $PI$ are shown in Fig. 1 (a), for a fixed depth $z = 5\,\mathrm{m}$. The curves $G(\gamma)/G_0$ at various depths, associated to a related vertical effective stress $\sigma'_{v0}$, for the soil type 1 having plasticity index $PI = 0$, are shown in Fig. 1 (b).

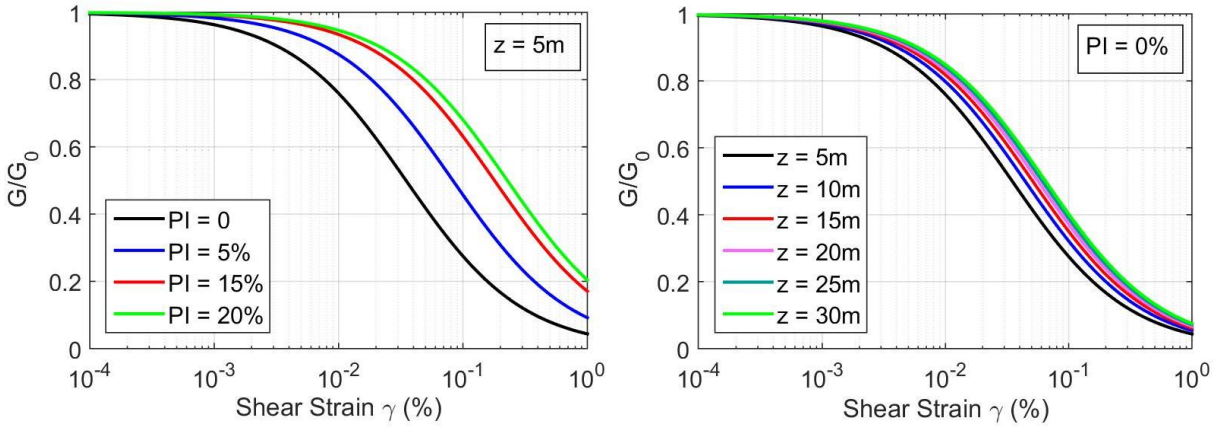


(a) (b)

Fig. 1. Normalized shear modulus reduction curves obtained by Darendeli formulation [33] (a) for the four soil types associated to different plasticity index $PI$ and a given depth $z = 5\,\mathrm{m}$,

158 (b) and for increasing depth $z$ and a given plasticity index $PI = 0$.

159

160 A set of 300 soil profiles is randomly generated with different layer thicknesses and
161 impedance contrasts, in order to represent various site conditions and estimate the influence of
162 their uncertainty on the amplification process. Among these 300 soil profiles, for 200 of
163 them, the shear wave velocity profile increases with depth to consider the effect of increasing
164 confining stresses. In the other 100 soil profiles, there is an inversion of the shear wave
165 velocity profile in one of the middle layers. The position and the thickness of the layer with
166 the shear wave velocity inversion are selected randomly.

167 The generated shear wave velocity profiles with depth $v_s(z)$ are shown in Fig. 2, in the cases
168 of increasing $v_s$ and of inversions in the profile (a and b, respectively). It can be noted that the
169 variability in the shear wave velocity profile, according to the same $v_{s,30} = 270\,\mathrm{m/s}$, can be
170 very large.

171

172 **2.2 Set of recorded seismic motions**

173 A set of 40 signals, recorded at rock outcrops, is selected as input for the computation of the
174 seismic wave propagation along the 300 generated soil profiles. These seismic motions
175 originate from ITACA, the Italian Strong Motion Database [34], ISESD, European Strong
176 Motion Database [35] or PEER, Pacific Earthquake Engineering Research Center Database
177 [36].

178 In the adopted set of seismic signals, 20 of them are representative of low to moderate
179 intensity with magnitudes ranging from 3 to 5.5 (associated to the type 2 response spectrum of
180 Eurocode 8 [25]) and the other 20 are representative of moderate to high seismicity with
181 magnitude ranging from 5.6 to 7.5 (type 1 response spectrum).

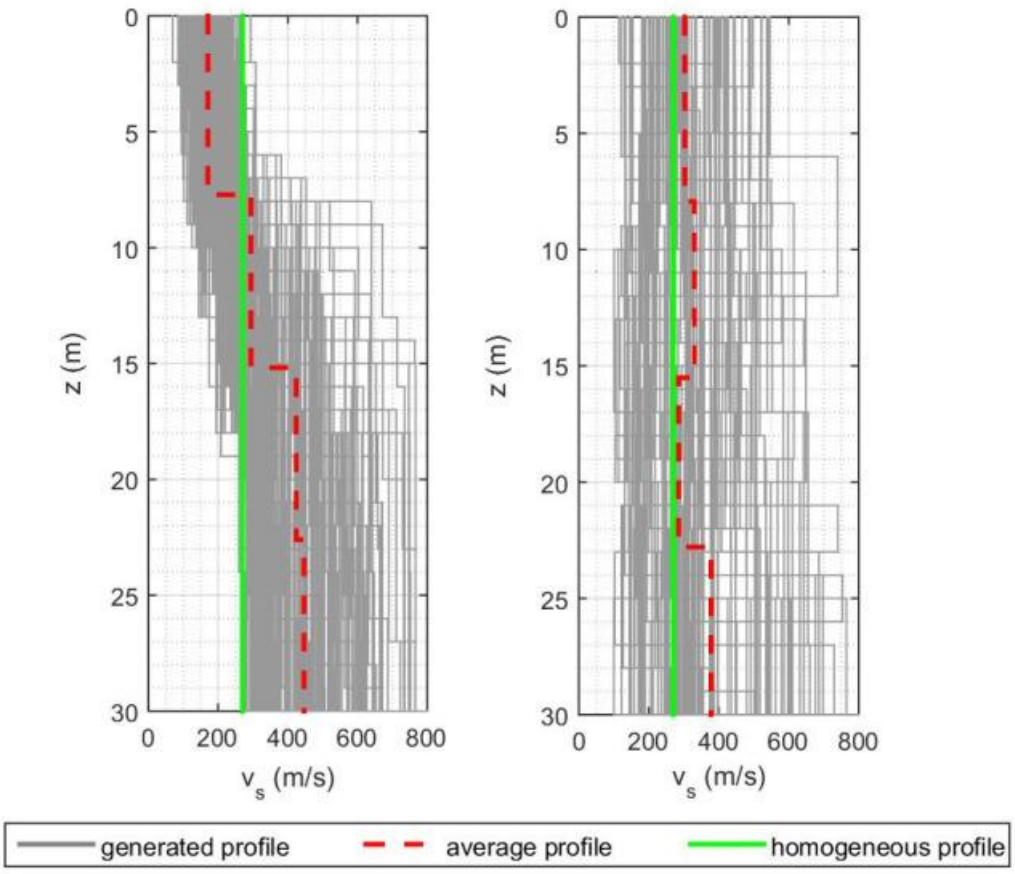


(a) (b)

Fig. 2. Generated shear wave velocity profiles with depth $v_s(z)$ in the cases of (a) increasing $v_s$ and (b) shear wave velocity inversion. All the generated soil profiles have the same average shear wave velocity $v_{s,30} = 270\,\mathrm{m/s}$.

Taking into account the influence of the frequency content on the free-field (FF) ground motion, the selected seismic records are representative of a wide variety of dominant frequencies. The set of recorded seismic motions is sorted in terms of frequency content using the equivalent period $T_{VA}$, parameter proposed by Cameron and Green [37], defined as

$$T_{VA} = 2\pi \frac{\alpha_V(\xi = 5\%)}{\alpha_A(\xi = 5\%)} \frac{v_{gR}}{a_{gR}} \tag{2}$$

where $a_{gR}$ and $v_{gR}$ are the peak ground acceleration and velocity at the outcrop, respectively.

The median spectrum amplification factors for horizontal motion are estimated by Newmark and Hall [38] as $\alpha_A(\xi=5\%)=2.12$ and $\alpha_V(\xi=5\%)=1.65$, for the constant acceleration and constant velocity regions of $5\%$ damped response spectra, respectively.

Fig. 3 shows the equivalent predominant frequency $1/T_{VA}$ related with the peak ground acceleration on rock outcrop $a_{gR}$ for the set of 40 seismic motions. The oblique lines represent uniform values of $v_{gR}$. The severity of seismic motion increases according to the direction of increasing velocity (from the bottom-right corner toward the top-left one, where the values of $a_{gR}$ and $v_{gR}$ are both higher). Based on the observations in Kobe [39], the values $a_{gR}=0.8\,\mathrm{g}$ and $v_{gR}=100\,\mathrm{cm/s}$ are considered as risk limits, meaning that the input motions above these values are considered as the most severe ones (Fig. 3). Then the set of the selected seismic motions is made up of a wide variety of frequency content, peak acceleration and peak velocity.

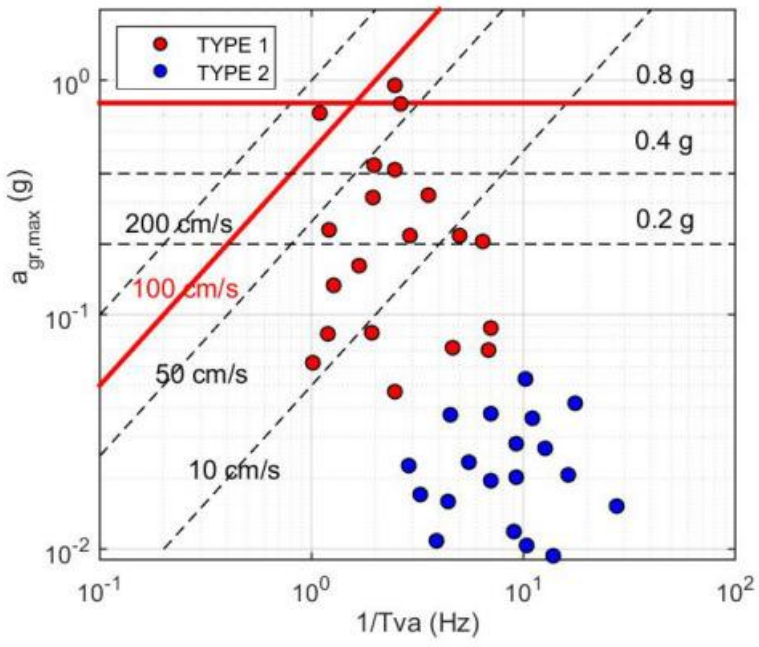


Fig. 3. Equivalent predominant frequency $T_{VA}$ related to the peak ground acceleration at the outcrop $a_{gR}$ for the set of 40 seismic motions. The oblique lines represent uniform values of

209 $v_{gR}$. The horizontal lines represent constant values of $a_{gR}$.

210

211 **2.3 Wave propagation model**

212 Assuming a vertical propagation in a horizontally layered medium, the numerical analysis is
213 undertaken as a one-dimensional approach. The soil is assumed homogeneous and both
214 assumptions of linear and nonlinear constitutive behavior are analyzed.

215 Quadratic line finite elements are adopted for spatial discretization and the Newmark
216 algorithm for time discretization, with some numerical damping. The SWAP_3C finite
217 element software [30,31,40,41] is used for the numerical simulations.

218 At the soil-bedrock interface, an absorbing boundary condition adopted by Joyner and Chen
219 [42] is applied in order to take into account the elasticity of the underlying bedrock and allow
220 energy to be radiated back. The mechanical properties characterizing the bedrock are the
221 density $\rho_b$ and the shear wave velocity $v_{sb}$.

222 The largest horizontal component of the signal recorded at the reference outcrop is halved and
223 imposed as the incident wave at the soil-bedrock interface.

224 The finite element size in each soil layer is defined as the minimum between 1m and one
225 tenth of the minimum wavelength, related to shear wave velocity in the layer and the
226 maximum frequency assumed equal to 15 Hz, above which the spectral content of the input
227 signal is considered negligible.

228 Details of the finite element model employed in this research are completely described by
229 Santisi d'Avila et al. [30,31].

230

231 **2.4 Hysteretic model for soil**

232 The so-called Masing-Prandtl-Ishlinskii-Iwan (MPII) nonlinear constitutive model [43] is
233 used for the soil in a total stress analysis. Its main feature is the satisfactory reproduction of

nonlinear and hysteretic behavior of soils under cyclic loadings [40,41], starting from the knowledge of a small number of parameters characterizing the soil properties, such as elastic parameters and the shear modulus redaction curve.

The MPII model is elasto-plastic with linear kinematic hardening. The plasticity model assumes an associated plastic flow, which allows for isotropic yield. This rheological model has no viscous damping and the soil damping is purely hysteretic and not frequency dependent. The size of the Von Mises yield surface is imposed by the backbone curve in the uniaxial stress case. The tangent constitutive matrix is deduced from the actual strain level and the strain and stress values at the previous time step [43,44].[44] This means that the stress level depends on the strain increment and strain history but not on the strain rate.

### 2.5 Data analysis

An optimal selection of site parameters is an important tool for the prediction of the expected ground motion. Based on recent results [14,22–24], the site dominant frequency $f_0$ and the shear wave velocity gradient $B_{30}$ are chosen as complementary proxies in this study.

As proposed by Regnier et al. [45], the shear wave velocity gradient $B_{30}$ is defined as the slope of the linear regression of the relation between the logarithm of the shear wave velocity profile $v_s(z)$ and the depth $z$. Thus, it is computed as:

$$\log\left(v_s(z)\right) = B_{30}\log(z) + A_{30} \pm \sigma_{30} \tag{3}$$

where $A_{30}$ is the vertical intercept of the regression, $\sigma_{30}$ is the standard deviation associated to the linear regression.

The shear wave velocity gradient $B_{30}$, estimated by Eq. (3) for all the generated 30 m deep soil profiles, quantifies the variation of the shear wave velocity $v_s(z)$ contrast in the superficial layers. Its value is close to zero if the velocity is nearly constant with depth and it

258 is larger if the shear wave velocity $v_s$ increases rapidly with depth [45].

259 The results of the numerical simulations of seismic wave propagation in the set of generated
260 soil profiles, are first analyzed in terms of amplification factors, according to Ciancimino et
261 al. [24], in both cases of linear and nonlinear soil behavior.

262 The soil amplification factor $S_s$ is a local indicator of the site amplification, providing an
263 estimate of the site effect on the FF motion. It is defined as the ratio of the peak ground
264 acceleration at the surface $a_g$ to the peak acceleration at the outcrop $a_{gR}$:

265 $$S_s = a_g / a_{gR} \tag{4}$$

266 The spectral amplification factor $SA$ and the spectral velocity factor $SV$ are used to quantify
267 the ground motion intensity in a given period range. These parameters are proposed by Rey et
268 al. [46]. They are defined as the ratio of $I_{soil}$ to $I_{rock}$. These are the intensity of the spectrum
269 estimated using the signal at the ground surface and at the outcrop, respectively. The
270 intensities used in the amplification factors $SA$ and $SV$ are calculated by Housner [47] using
271 the spectrum in terms of acceleration $PSA(T)$ and velocity $PSV(T)$, respectively, as
272 follows:

273 $$SA = \frac{I_{soil}}{I_{rock}} \quad \text{with} \quad I = \int_{T_1}^{T_2} PSA(T)\,dT \tag{5}$$

274 $$SV = \frac{I_{soil}}{I_{rock}} \quad \text{with} \quad I = \int_{T_1}^{T_2} PSV(T)\,dT \tag{6}$$

275 In Eqs (5) and (6), $[T_1 - T_2]$ is the fixed range of vibration period.

276 In this research, the spectra $PSA(T)$ and $PSV(T)$ are normalized with respect to the peak
277 acceleration at the outcrop $a_{gR}$. The period range $[0.05 - 2.5\text{s}]$, representative of the
278 fundamental vibration period for more common structures, is divided into three sub-ranges in
279 order to analyze the results for short, middle and long periods of vibration. Spectral

amplification factors for short $[0.05-0.5\text{s}]$, middle $[0.5-1\text{s}]$ and long $[1-2.5\text{s}]$ periods of vibration are indicated as $(SA_S, SV_S)$, $(SA_M, SV_M)$ and $(SA_L, SV_L)$, respectively.

In a second phase, the response spectra of numerical FF motion are compared to those suggested by Eurocode 8 [25]. Finally, the results in terms of site amplification factors are compared with the Eurocode 8 [25], the New Zealand Standard [26] building codes, and those evaluated by Pitilakis et al. [18], Ciancimino et al. [24].

## 3. Results and discussion

The variability of the shear wave velocity profiles with depth $v_s(z)$ for the set of generated soil profiles, having the same average $v_{s,30} = 270\,\text{m/s}$, is shown in Fig. 2. The FF motion obtained by numerical simulation, propagating the set of recorded seismic signals along the generated soil profiles is analyzed.

In the following, the influence on site amplification of complementary parameters as the shear wave velocity profiles with depth $v_s(z)$, the site dominant frequency $f_0$ and the shear wave velocity gradient $B_{30}$ is assessed. The fluctuation of amplification factors with the site parameters $f_0$ and $B_{30}$ is analyzed.

### 3.1 Site parameter variability

The dominant frequency of the site $f_0$ is obtained by evaluating the FF to bedrock transfer function (TF) that is the ratio of the Fourier spectrum of the accelerograms at the FF soil surface and at the outcropping bedrock surface. A low-amplitude signal is used so that the soil remains in the elastic regime. The frequency corresponding to the peak of this TF corresponds to the fundamental frequency of the soil column, considered as the dominant frequency of the site $f_0$. In the case of a homogeneous soil, the fundamental frequency of a 30 m deep soil

304 profile, having a shear wave velocity $v_s = 270\,\mathrm{m/s}$ , is also deduced [48] as
305 $f_0 = v_s/(4H) = 2.25\,\mathrm{Hz}$ . The homogeneous soil profile is adopted in the following
306 comparisons as canonical case.
307 Fig. 4 displays the TF obtained for the soil profile with a homogeneous soil, the generated soil
308 profiles with increasing shear wave velocity with depth $v_s(z)$ and those with an inversion in
309 the $v_s(z)$ profile. The dominant frequency of the site $f_0$, obtained for the set of all the
310 generated soil profiles ranges from 1.5 to 3.5Hz. For increasing $v_s(z)$ profiles (Fig. 4a), the
311 dominant frequency of the site is mostly higher than the frequency for the homogeneous case.
312 Whereas the natural frequencies obtained for soil profiles with an inversion in $v_s(z)$ are
313 distributed in a frequency range (Fig. 4b). The peaks of the TF obtained for the generated soil
314 profiles show a higher amplification compared with the homogeneous soil profile in most
315 cases. In particular, the amplification estimated for the soil profiles having increasing $v_s(z)$ is
316 larger for higher $f_0$ (Fig. 4a).
317 According to Fig. 4, the site amplification changes depending on the stratigraphy (i.e. shear
318 wave profile with depth $v_s(z)$) and the fundamental frequency of the site $f_0$. The frequency
319 content of the surface motion varies accordingly.
320 Fig. 5 illustrates the linear correlation between the shear wave velocity gradient $B_{30}$ and the
321 fundamental frequency of the site $f_0$, for the set of generated soil profiles with given $v_{s,30}$.
322 This correlation is high, with a correlation coefficient $r^2 = 0.85$, for the whole set of 300 soil
323 profiles.
324 The amplification factors in Eqs (4), (5) and (6) are calculated using the computed FF motion
325 and the related response spectrum for all the 24000 samples (set of 40 recorded seismic
326 signals applied to 300 generated soil profiles, for linear and nonlinear soil behaviors).

The estimated amplification factors $S_s$, $SA$ and $SV$, $SA_S$, $SA_M$ and $SA_L$, $SV_S$, $SV_M$ and $SV_L$, are shown in Figs 6, 7, 8, and 9 as functions of the dominant period of the site $T_0 = 1/f_0$ and of the shear wave velocity gradient $B_{30}$, respectively, for both cases of linear (a) and nonlinear (b) behavior. The trend of mean and standard deviation is also displayed by the thick and dashed lines, respectively.

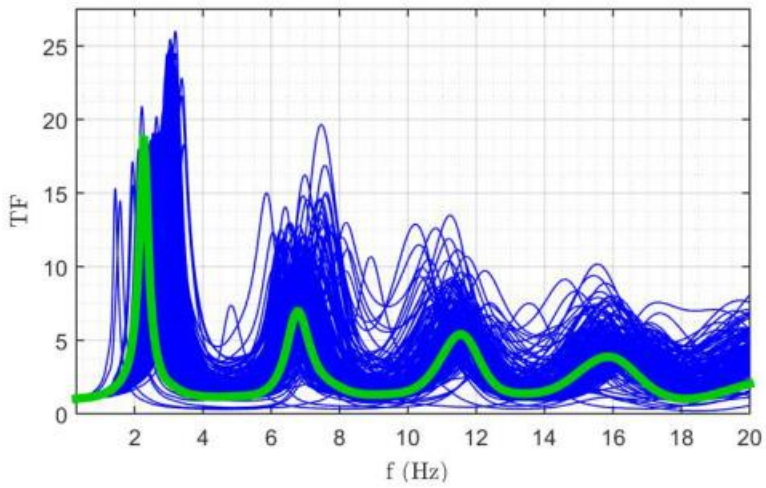


(a)

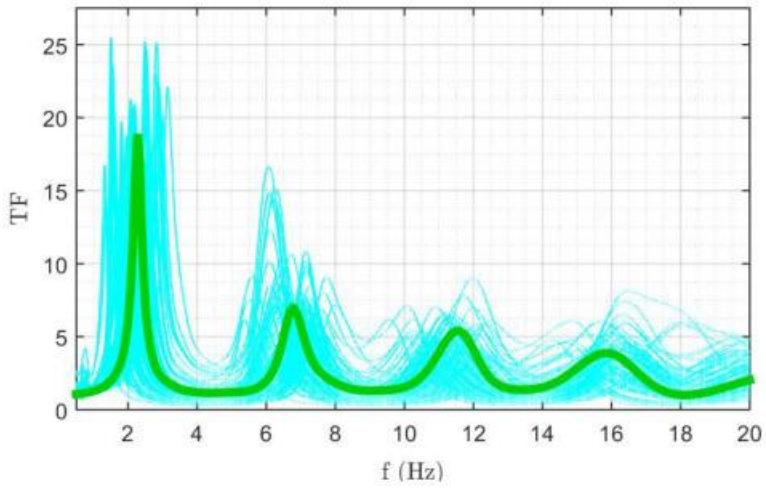


(b)

Fig. 4. Free-field to bedrock transfer function for the generated deep soil profiles having increasing shear wave velocity profile (a) and showing a velocity inversion (b). The thick line is the transfer function for the homogeneous soil profile.

Figs 6, 7, 8 and 9 illustrate the amplification factors in the three fixed ranges of period in order to understand if their variation is modified for different periods. It appears that the largest amplifications are reached for short vibration periods (lower than $0.5\,\mathrm{s}$).

Figs 6 and 8 display that site amplification is strongly dependent on the site predominant period $T_0$, for short vibration periods of the FF motion $(SA_S, SV_S)$ and independent from it for long periods $(SA_L, SV_L)$. Moreover, site amplification is much more pronounced in soil profiles having $T_0$ lower than that of the homogeneous profile, for short vibration periods of the FF motion $(SA_S, SV_S)$. Whereas, for middle periods of vibrations $(SA_M, SV_M)$, site amplification is more pronounced in soil profiles having predominant period $T_0$ higher than that of the homogeneous profile.

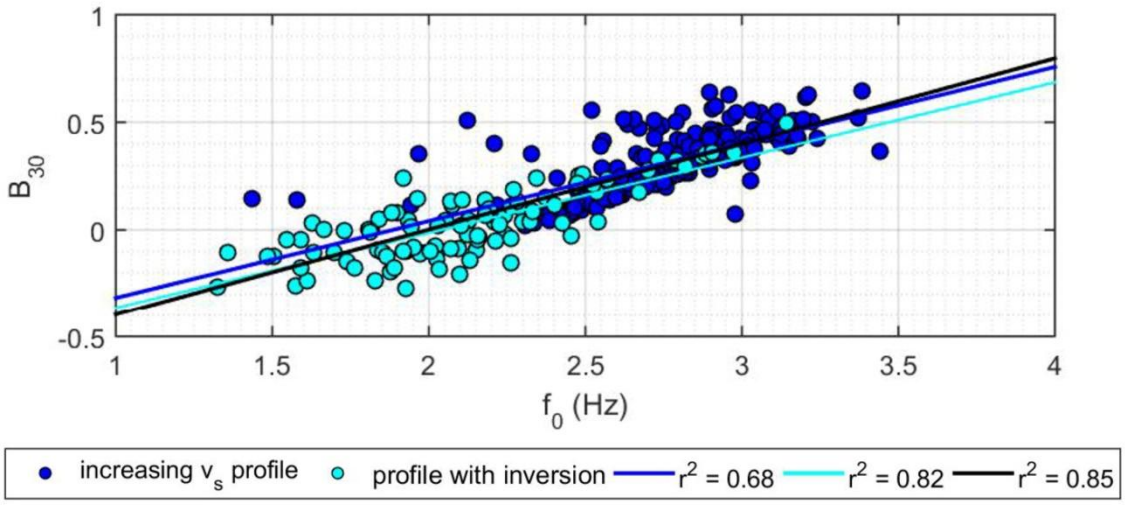


Fig. 5. Linear regression of the shear wave velocity gradient $B_{30}$ with reference to the fundamental frequency of the site $f_0$, for the generated deep soil profiles. The thick line is for the set of all 300 generated soil profiles.

Figs 7 and 9 show that the largest values of amplification factors are reached for short

vibration periods of the FF motion $(SA_S, SV_S)$, lower than $0.5\,\mathrm{s}$, in soil profiles having a high shear wave velocity gradient $B_{30}$, which corresponds to sites with a large impedance contrast in the first $30\,\mathrm{m}$ or with a steep slope in shear wave velocity profile.

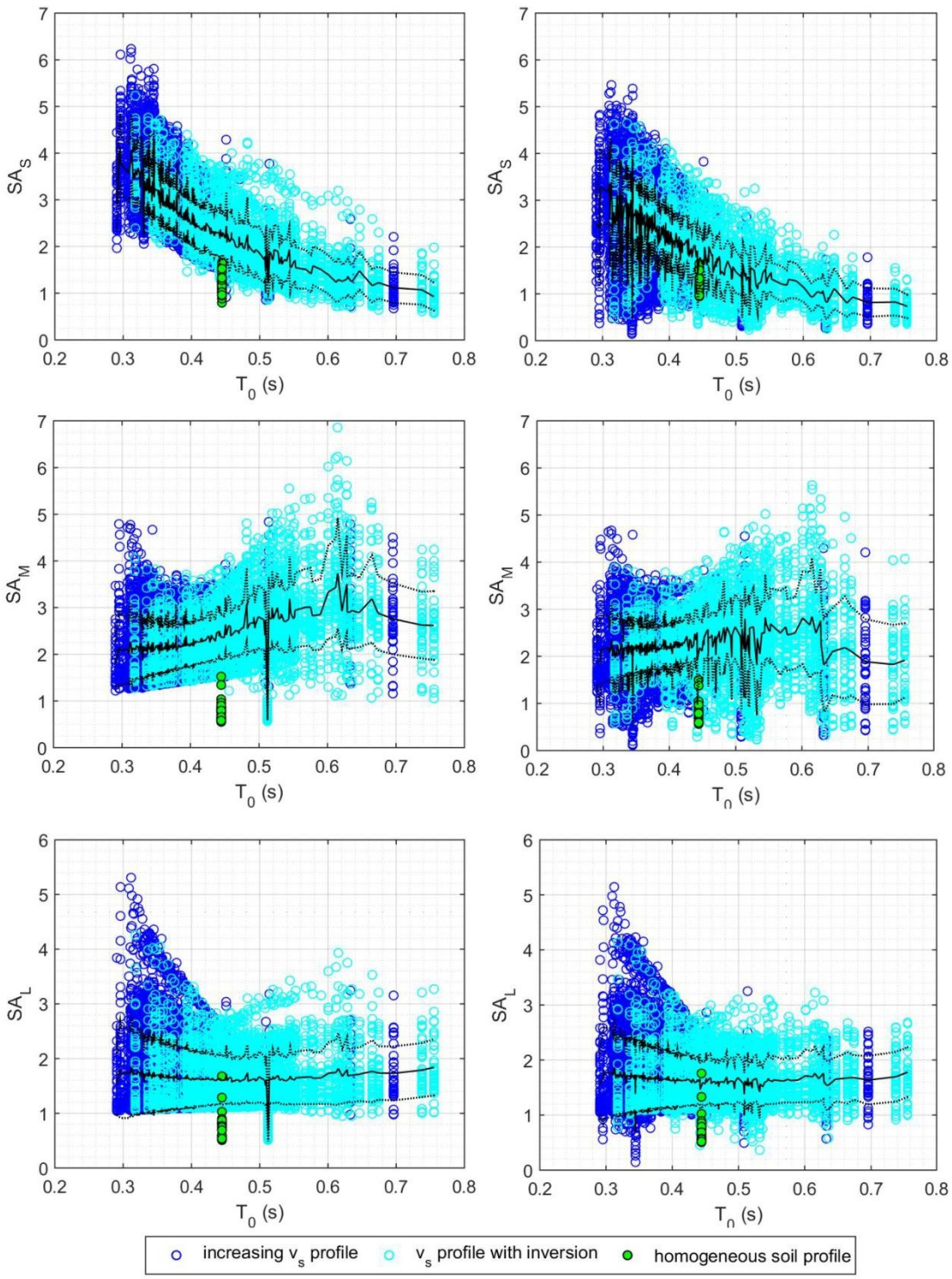


(a) (b)

Fig. 6. Amplification factors $SA_S$, $SA_M$ and $SA_L$ as a function of the dominant period of the site $T_0$, for both cases of linear (a) and nonlinear (b) behaviors. The thick and dashed lines represent the mean and means plus one standard deviation (SD) trend.

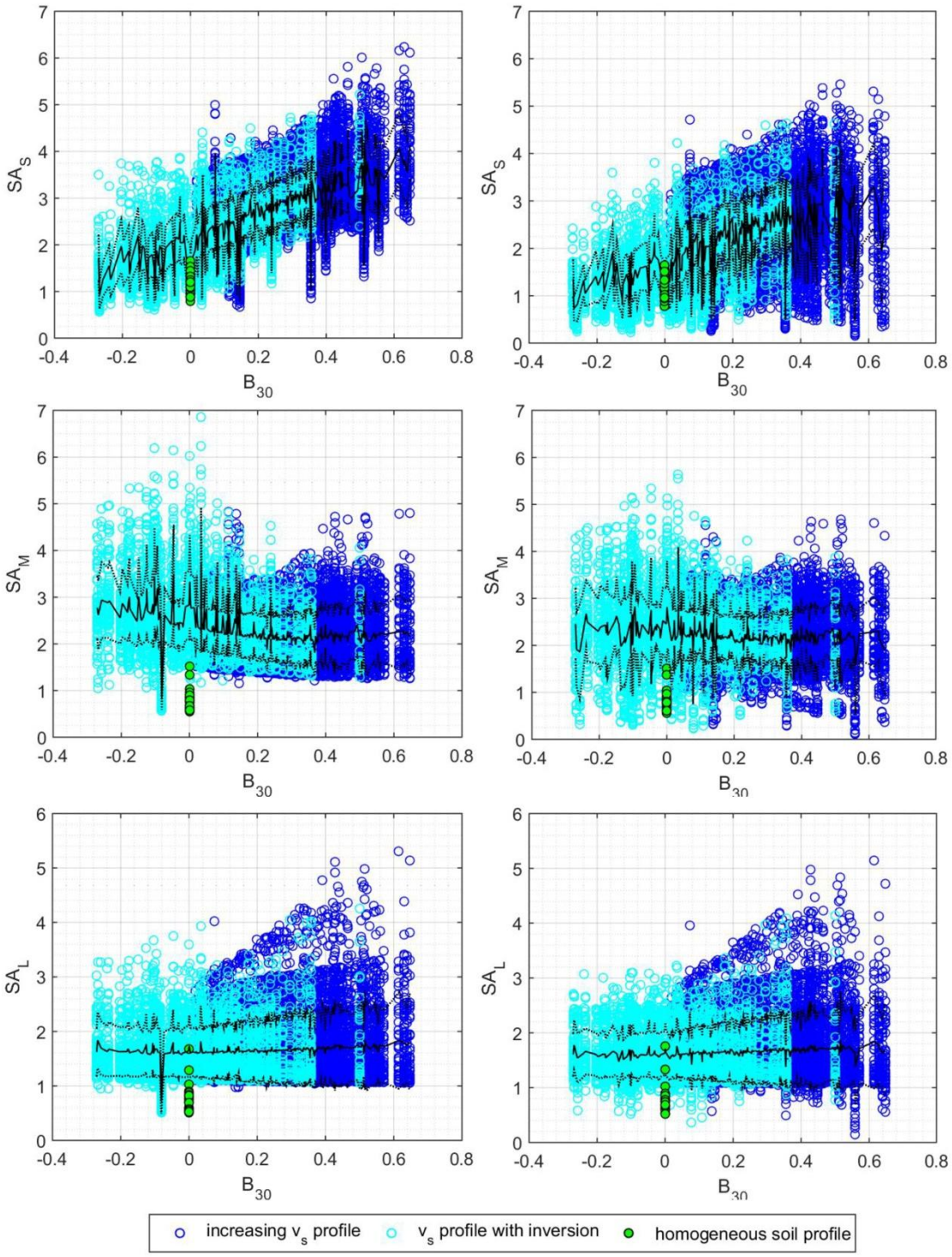


(a) (b)

Fig. 7. Amplification factors $SA_S$, $SA_M$ and $SA_L$ as a function of the shear wave velocity gradient $B_{30}$, for both cases of linear (a) and nonlinear (b) behaviors. The thick and dashed lines represent the mean and means plus one standard deviation (SD) trend.

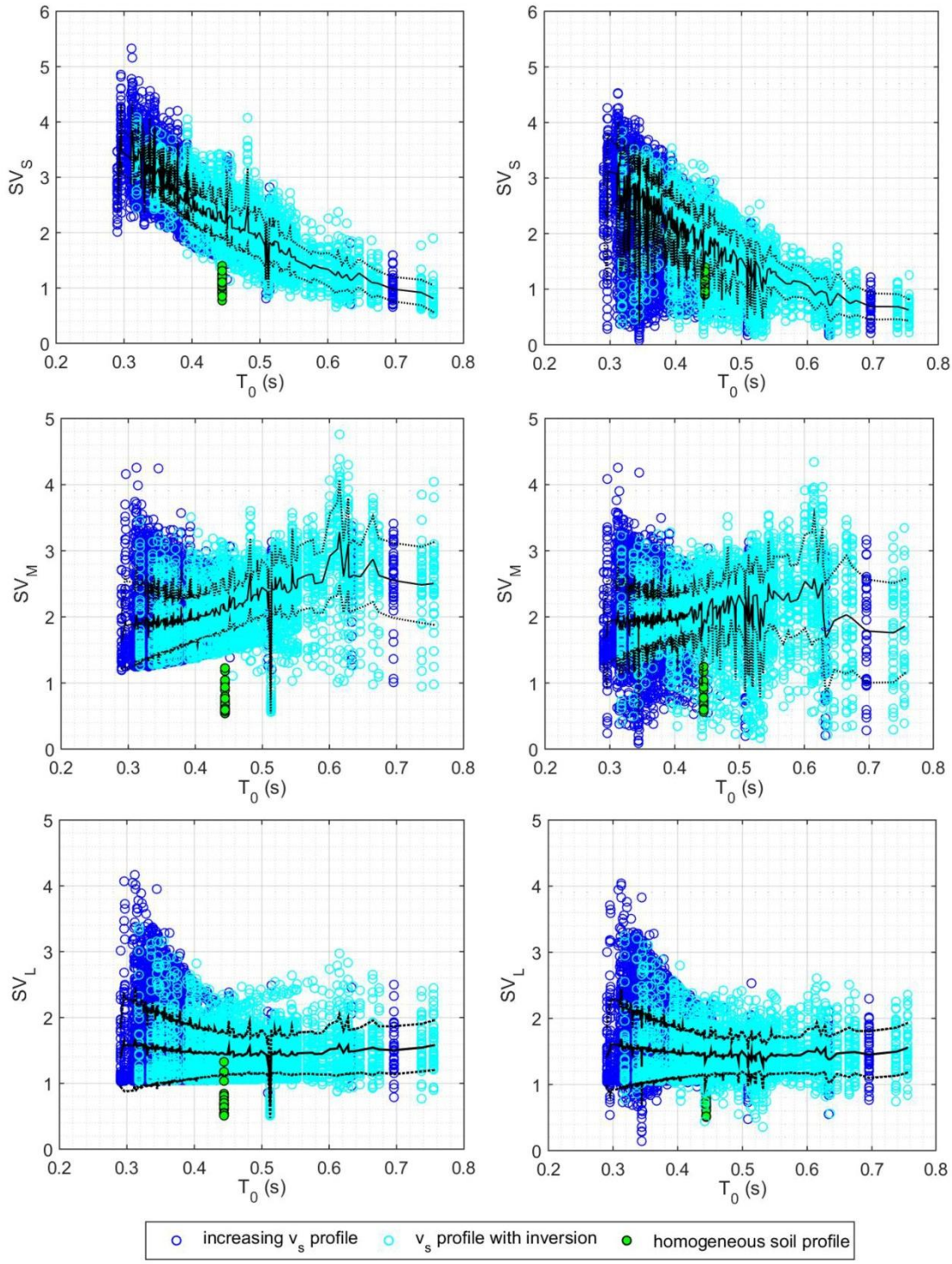


(a) (b)

Fig. 8. Amplification factors $SV_S$, $SV_M$ and $SV_L$ as a function of the dominant period of the site $T_0$, for both cases of linear (a) and nonlinear (b) behaviors. The thick and dashed lines represent the mean and means plus one standard deviation (SD) trend.

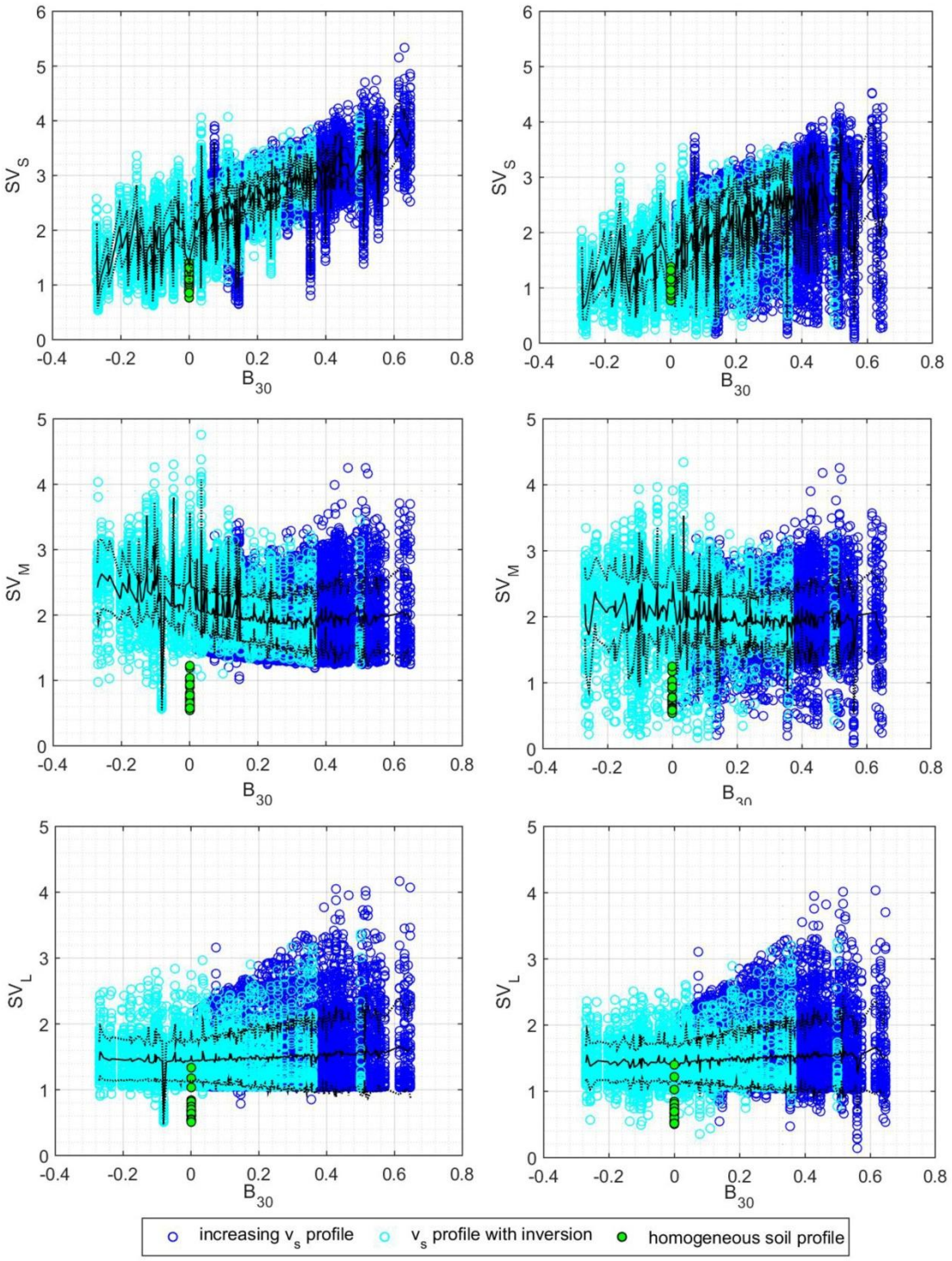


(a) (b)

Fig. 9. Amplification factors $SV_S$, $SV_M$ and $SV_L$ as a function of the shear wave velocity gradient $B_{30}$, for both cases of linear (a) and nonlinear (b) behaviors. The thick and dashed lines represent the mean and means plus one standard deviation (SD) trend.

The nonlinear soil behavior on the site response induces a reduced amplification effect. Similarly to the case of linear soil behavior, the site amplification is more pronounced in the case of short vibration periods of the FF motion and it is strongly dependent on the proposed site parameters. On the contrary, the site amplification is less pronounced and independent from the proposed site parameters, for longer vibration periods of the FF motion.

### 3.2 Influence on site effects of the nonlinear soil behavior

In this section, the effects of soil nonlinearities on site response are investigated with reference to the proposed site proxies (predominant period $T_0$ and shear wave velocity gradient $B_{30}$). The main goal is to verify the reliability of $T_0$ and $B_{30}$ even in the range of soil nonlinear behavior. The impact of nonlinear soil response on the site response is characterized in terms of amplification factor SV. The SV factor is estimated in both cases of linear and nonlinear soil response, in the three adopted period ranges. The amplification factor $NL/L$ is computed as the ratio of spectral velocity factors $SV_S$, $SV_M$ and $SV_L$ in the ranges of short, middle and long period, for nonlinear soil behavior to that for linear soil behavior.

Fig.10 illustrates the average amplification factor as a function of the site dominant period $T_0$ (Fig. 10a) and shear wave velocity gradient $B_{30}$ (Fig. 10b). Results are distinguished between those for weak earthquakes (associated to the type 2 response spectrum of Eurocode 8 [25]) and strong earthquakes (type 1 response spectrum).

As expected, the effect of nonlinear soil behavior is negligible for small earthquakes (type 2 response spectrum of Eurocode 8 [25]) for the whole range of periods of vibration. In fact, the

400 $NL/L$ ratio is close to one.

401 In the case of stronger earthquakes (type 1 response spectrum), the modification in the site
402 response depends on the stratigraphy and varies with the vibration period of the FF motion.

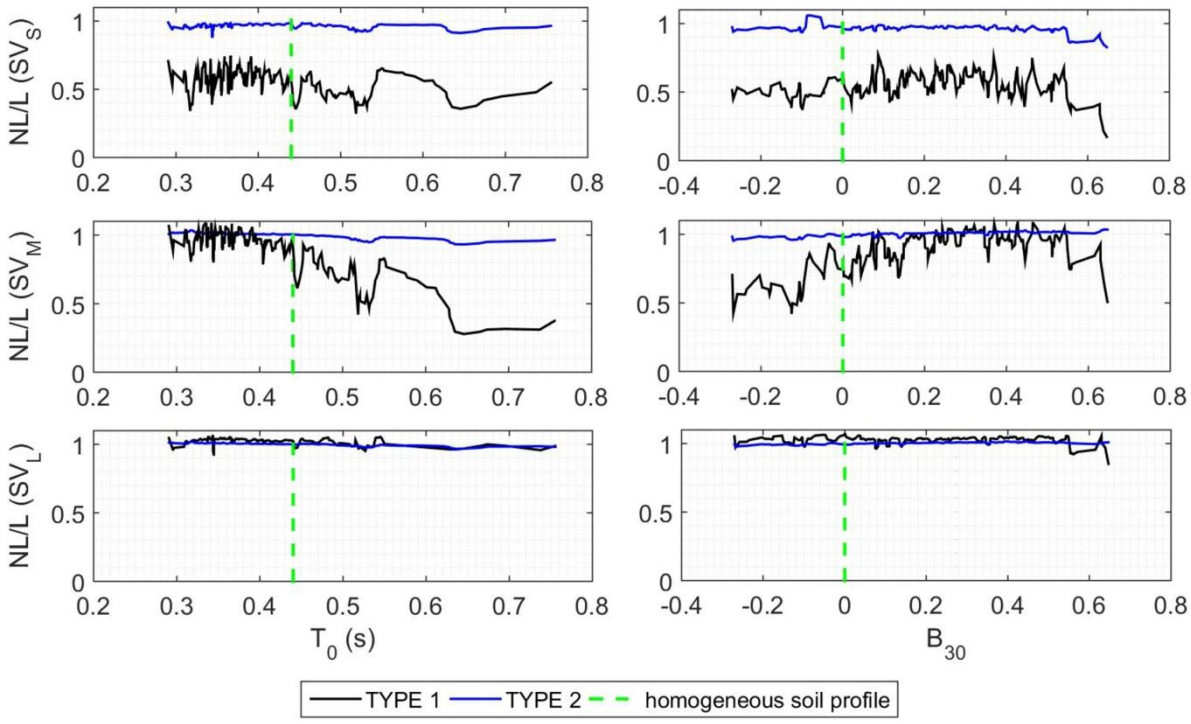


403

404 (a) (b)

405 Fig. 10. Computed ratio of spectral velocity factors $SV_S$, $SV_M$ and $SV_L$ (short, intermediate
406 and long periods of vibration) for nonlinear soil behavior to that for linear soil behavior
407 (*NL/L*) as a function of the dominant period of the site $T_0$ (a) and the shear wave velocity
408 gradient $B_{30}$ (b), for the whole set of generated soil profiles. The curves are distinguished
409 between those for small earthquakes (associated to the type 2 response spectrum of Eurocode
410 8) and strong earthquakes (type 1 response spectrum).

411

412 According to Fig. 10, for vibration periods of the strong motion over 1s, the effect of
413 nonlinear soil behavior is negligible (see $SV_L$). On the contrary, in the range of short periods
414 (see $SV_S$), the amplitude reduction due to nonlinear effects is up to 60%. Moreover, the

amplification factor in the range of middle periods (see $SV_M$) show a remarkable amplitude reduction for a site predominant period $T_0$ higher than $0.44\text{s}$ (period of vibration of the homogeneous soil profile) and a reduction up to 10% for lower periods $T_0$ (Fig 10a). An important amplitude reduction is obtained for a shear wave velocity gradient $B_{30}$ outside the range $[0-0.5]$, that correspond to soil profiles with significant impedance contrast (high $B_{30}$) and velocity inversions (negative $B_{30}$).

### 3.4 Comparison with building codes

Fig. 11 displays the comparison of the average pseudo-acceleration response spectrum normalized with respect to the peak acceleration of the outcropping motion, using a damping ratio of $5\%$.

The linear and nonlinear computations are separated and, for both, the cases of weak earthquakes (associated to the type 2 response spectrum of the Eurocode 8 [25]) and strong earthquakes (type 1 response spectrum) are distinguished. In each of these combinations, the average pseudo-acceleration response spectra are estimated for the FF motion in the case of increasing shear wave velocity and for profiles with a velocity inversion.

The elastic response spectra proposed by Eurocode 8 is conservative, compared to the obtained average response spectra, for higher periods (higher than $0.2\text{s}$ for type 2 and $0.6\text{s}$ for type 1). Conversely, for lower periods, the average response spectrum, obtained for all the generated soil profiles, gives higher acceleration peaks.

If the elastic response spectrum proposed by Eurocode 8 [3] is compared for the spectrum in the homogeneous case, with average soil properties, it is conservative for the whole ranges of period for weak earthquakes (type 2) and in most cases for strong earthquakes (type 1).

The reduction of the site response for the nonlinear soil behavior is negligible for weak

earthquakes (type 2) and significant for strong earthquakes (type 1).

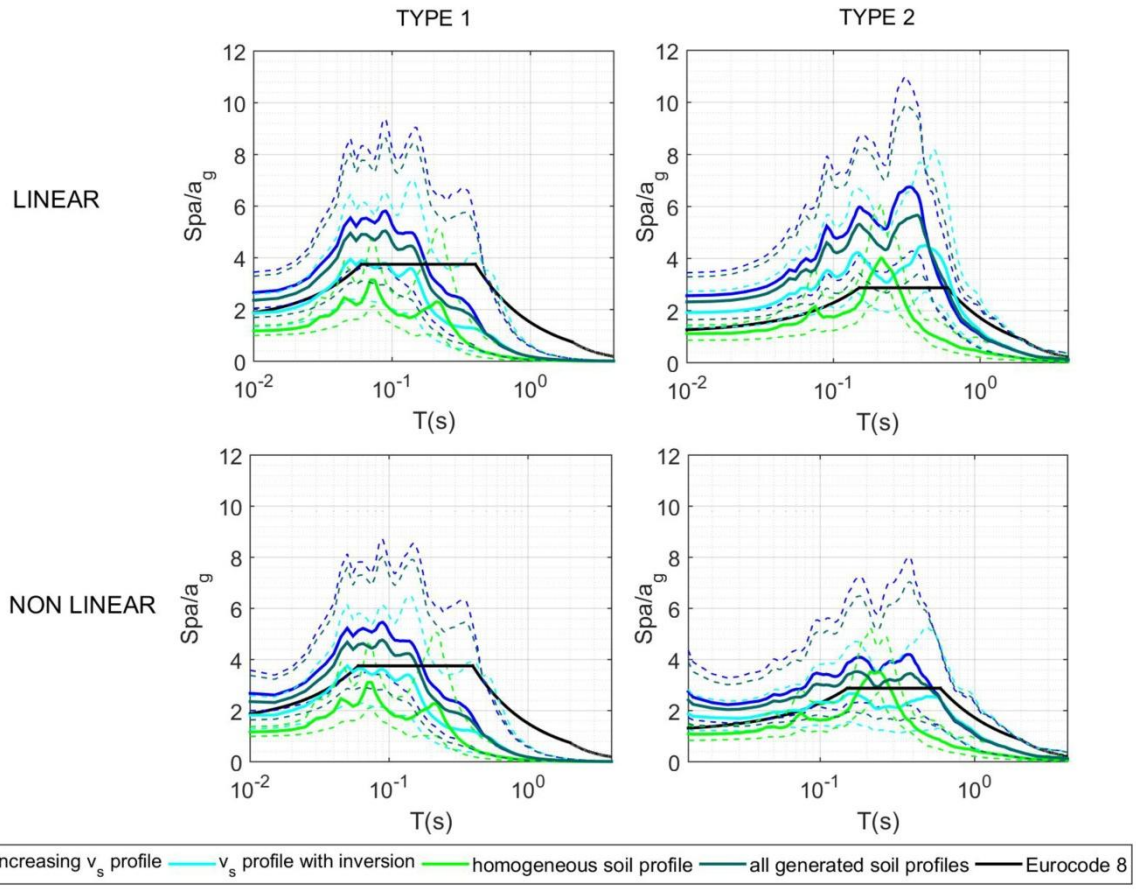


(a) (b)

Fig. 11. Mean (solid line) acceleration response spectra (damping ratio of 5%) and mean plus one standard deviation (dashed line), evaluated for the free-field motion of the generated multilayered soil profiles, compared to the homogeneous case and the elastic response spectrum proposed by Eurocode 8 [3]. The cases are distinguished as follows: assumption of linear and nonlinear soil behavior; weak earthquakes (a) and strong earthquakes (b).

Following the approach adopted by Ciancimino et al. [24] for the linear regime, the site amplification factors are evaluated for the samples of the present statistical analysis, in the case of linear and nonlinear soil behavior. The computed amplification factors are compared with those suggested by Eurocode 8 [25] and New Zealand Standard [26] building codes, with those proposed by Pitilakis et al. [18] and with those obtained by Ciancimino et al. [24]. The ground type classification used in the Eurocode 8 [25] is only based on the $v_{s,30}$ parameter. In

453 the New Zealand Standard [26], the fundamental site period is included as a proxy of site
454 effects. In addition, Pitilakis et al. [18] classify the ground type using the fundamental period
455 of the site, the depth of the seismic bedrock and the average soil column shear wave velocity
456 are taken into account. The 300 generated soil profiles are identified as ground type C
457 according to Eurocode 8 [25] and as C2 according Pitilakis et al. [18]. Among them, 286 are
458 identified as ground type C according to the New Zealand Standard [26] building codes
459 $(T_0 > 0.6s)$.

460 The comparison between the mean value of site amplification factors $S_s$ (Eq. (4)) and $SA$
461 (Eq. (5)), and the values within one standard deviation of the mean are represented in Fig. 12
462 for weak earthquakes and in Fig. 13 for strong earthquakes. These values are compared to
463 those obtained according to the building codes to analyze their reliability. The coefficient of
464 variation $CV$ of $S_s$ and $SA$ is also calculated. In each figure, the simulations under the
465 assumption of linear and nonlinear soil behavior are separated. The amplification factors are
466 estimated, for both soil behaviors, using only the FF motions of multilayered soil profiles with
467 increasing shear wave velocity with depth, only the FF motions of soil profiles with a velocity
468 inversion, the FF motions of all the generated soil profiles and the FF motion of the
469 homogeneous soil profile.

470 The obtained numerical results obtained under the assumption of linear soil behavior are also
471 compared to those obtained by Ciancimino et al. [24], that performed analyses on a database
472 of seismic responses of one-dimensional soil profiles having equivalent linear behavior. We
473 can observe that our results under the assumption of linear behavior are in good agreement
474 with those obtained by Ciancimino et al. [24].

475 According to Figs 12 and 13, only the amplification factors obtained for the case of
476 homogeneous soil profile are smaller than those suggested by Eurocode 8 [25] and the same
477 consideration is made comparing with the New Zealand Standard [26] building codes (Fig.

14).

It is interesting to note that the values proposed by Pitilakis et al. [18] for the site amplification factor $SA$ are close to those computed using the set of generated samples in the present analysis. Conversely, the values proposed by Pitilakis et al. [18] for the site amplification factor $S_s$ are lower than those obtained in the present research. This means that ground classification based on complementary site proxies instead on a single proxy is more adequate. But also it is important to understand the best complementary proxies that allow predicting the site response for different ranges of periods.

Moreover, the nonlinear effects are negligible in terms of mean values and $CV$ of the amplification factors, for weak earthquakes (Fig. 12) and they are significant for strong earthquakes (Fig. 13).

The average amplification factors obtained for soil profiles with a velocity inversion are lower than the ones associated to other soil profiles.

Lastly, Fig. 14 shows that the comparison between the computed amplification factors and those deduced by New Zealand Standard [26]. The difference observed could be justified by a higher seismicity expected in New Zealand that could increase the effect of nonlinear soil behavior and thus reduce the peak acceleration.

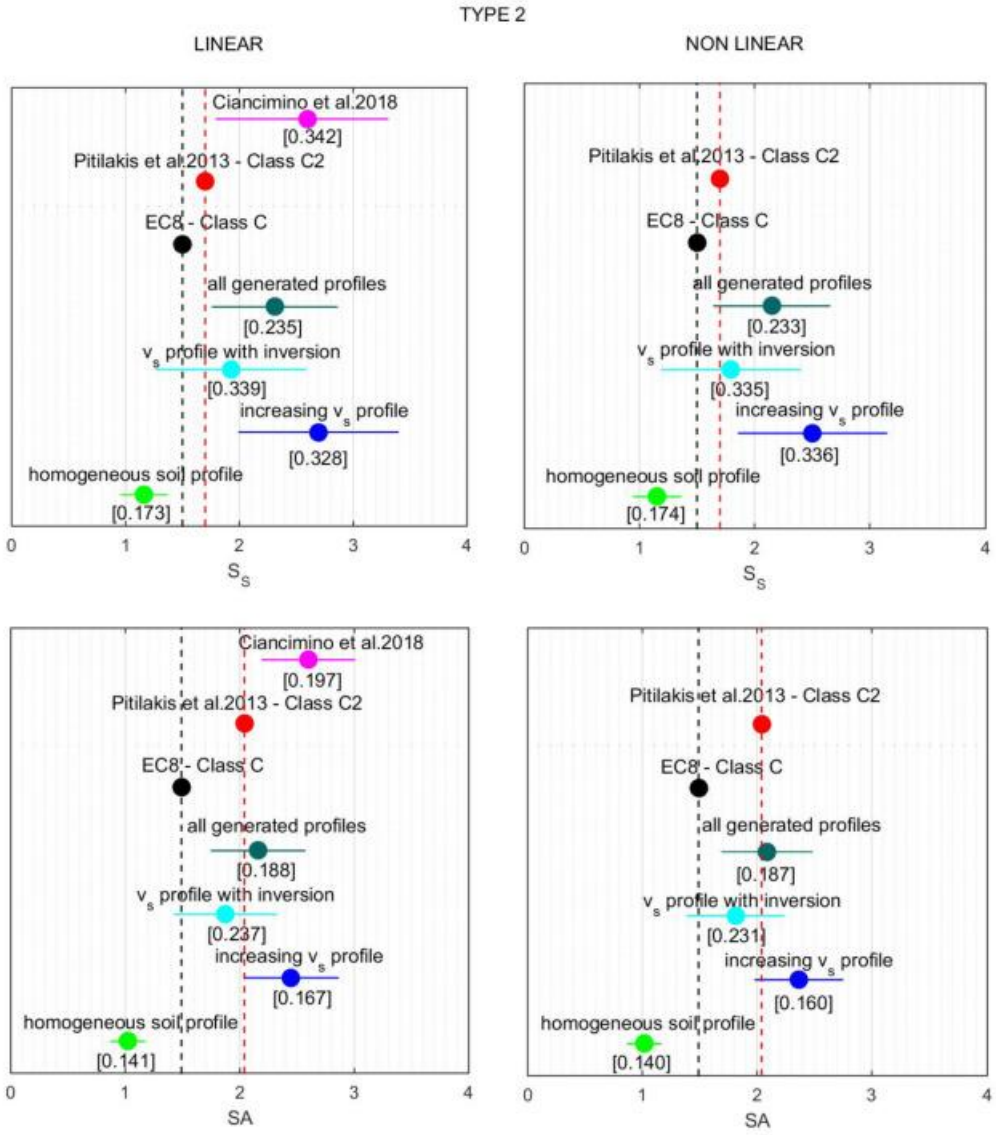


(a) (b)

Fig. 12. Mean value of site amplification factors $S_s$ (top) and *SA* (bottom), the values within one standard deviation of the mean and the coefficient of variation *CV* (value between brackets) in the case of small earthquakes (type 2 response spectrum of Eurocode 8 [25]), for numerical simulations under the assumption of linear (a) and nonlinear (b) soil behavior. The values suggested by Eurocode 8 [25], Pitilakis et al. [18] and Ciancimino et al [24] are indicated.

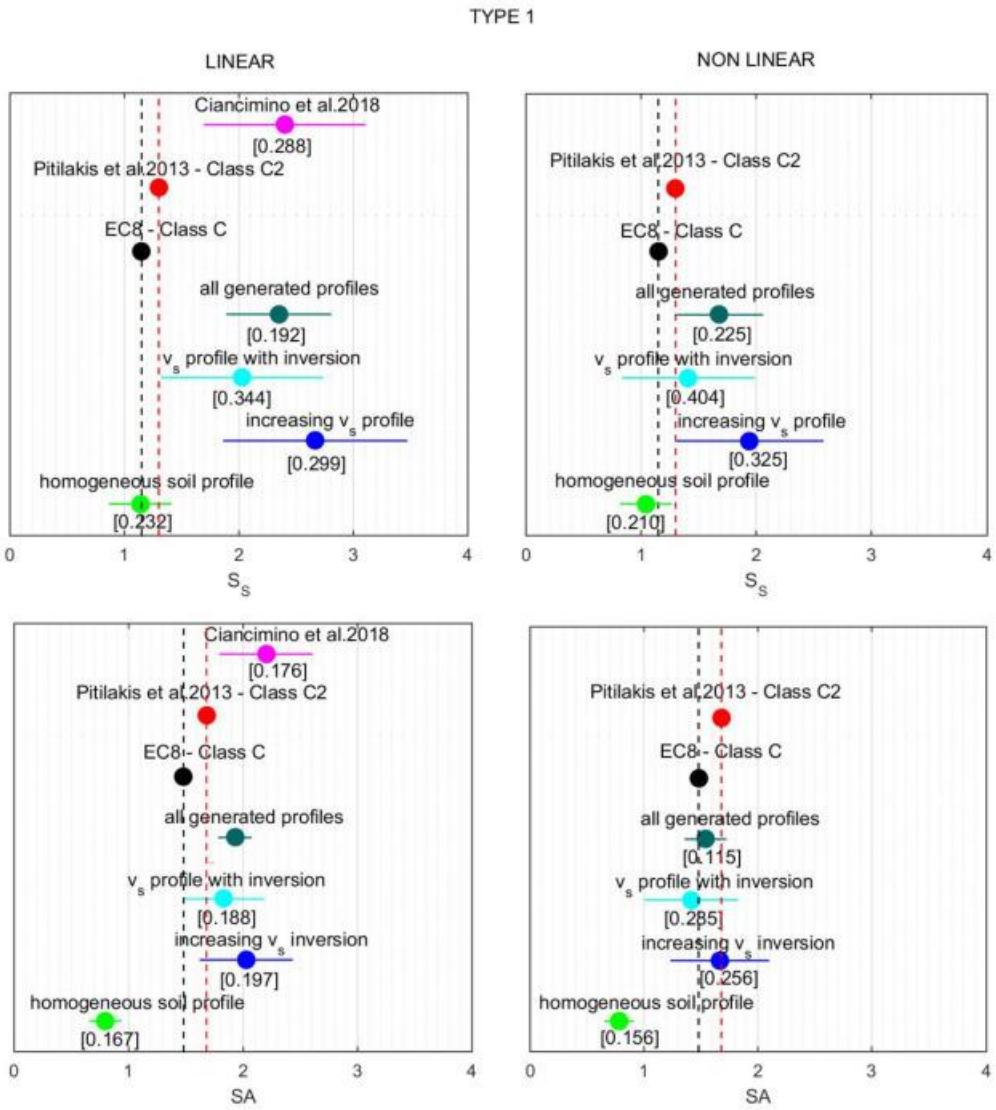


(a) (b)

Fig. 13. Mean value of site amplification factors $S_s$ (top) and *SA* (bottom), the values within one standard deviation of the mean and the coefficient of variation *CV* (value between brackets) in the case of strong earthquakes (type 1 response spectrum of Eurocode 8 [25]), for numerical simulations under the assumption of linear (a) and nonlinear (b) soil behavior. The values suggested by Eurocode 8 [25], Pitilakis et al. [18] and Ciancimino et al [24] are indicated.

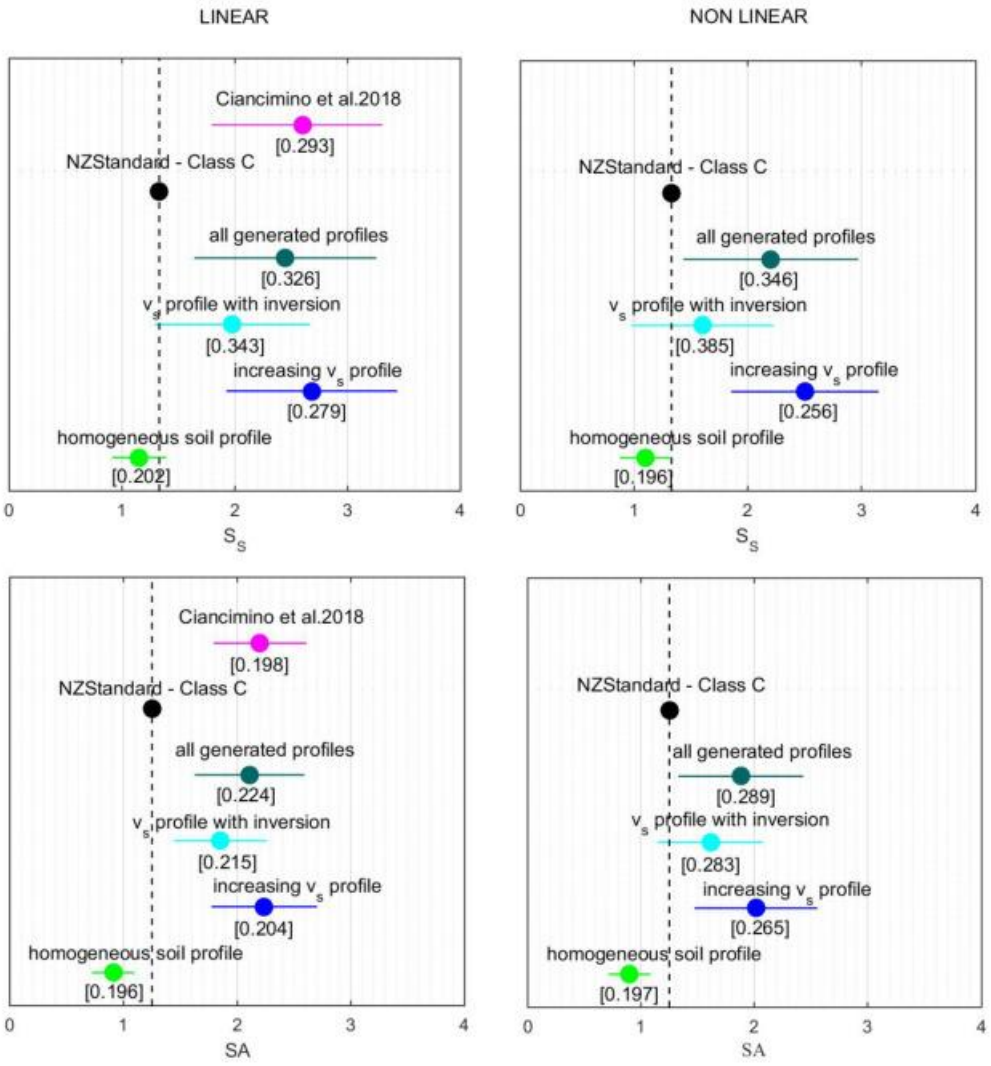


(a) (b)

Fig. 14. Mean value of site amplification factors $S_s$ (top) and *SA* (bottom), the values within one standard deviation of the mean and the coefficient of variation *CV* (value between brackets) for the whole set of recorded seismic signals. Numerical simulations under the assumption of linear (a) and nonlinear (b) soil behavior are separated. The values suggested by the New Zealand Standard [26] building codes are indicated.

## 4. Conclusions

The vertical propagation of various recorded seismic signals along stochastically generated soil profiles is numerically simulated to obtain the FF motion, in both cases of linear and

522 nonlinear soil behavior. The average shear wave velocity in the upper 30 m of soil profiles
523 $v_{s,30}$ is fixed and corresponds to the ground type C, according to the Eurocode 8. The soil-
524 bedrock interface depth is selected as $H_{800} = 30\,\text{m}$.
525 This research highlights the influence of the layering uncertainty on the site response. It is
526 demonstrated that the average shear wave velocity $v_{s,30}$ is not able, as single parameter, to
527 characterize the soil profiles in terms of expected amplification level over the whole
528 frequency range.
529 Two site parameters are proposed as proxies, complementary to $v_{s,30}$, such as the dominant
530 frequency of the site $f_0$ and the shear wave velocity gradient $B_{30}$. The site response is
531 represented in terms of site amplification factors, deduced using the response spectrum of the
532 FF motion, for the 24000 performed simulations (set of 40 recorded seismic signals applied to
533 300 generated soil profiles, for linear and nonlinear soil behaviors). The influence on site
534 amplification of the shear wave velocity profile, site dominant frequency and shear wave
535 velocity gradient are analyzed independently from $H_{800}$.
536 The obtained amplification factors are functions of both site conditions and intensity of rock
537 motions and the values could decrease due to soil nonlinearity. The amplification factors
538 increase with decreasing site dominant period $T_0$ and increasing shear wave velocity gradient
539 $B_{30}$, when they are evaluated over a large range of vibration periods $[0.05-2.5\text{s}]$.
540 Nevertheless, site amplification appears strongly dependent on the site predominant period
541 $T_0$, for short vibration periods of the FF motion and independent from it for long periods.
542 Moreover, site amplification is much more pronounced in soil profiles having $T_0$ lower than
543 that of the homogeneous profile, for short vibration periods of the FF motion.
544 The largest values of amplification factors are reached for short vibration periods of the FF
545 motion, lower than $0.5\text{s}$, in soil profiles having a high shear wave velocity gradient $B_{30}$,

546 which corresponds to sites with a large impedance contrast in the first 30 m or with a steep
547 slope in the shear wave velocity profile.
548 The site response is modified when the nonlinear soil behavior is taken into account in the
549 numerical simulations. The nonlinear soil behavior on the site response induces a reduced
550 amplification effect. Similarly to the case of linear soil behavior, the site amplification is more
551 pronounced in the case of short vibration periods of the FF motion and it is strongly
552 dependent on the proposed site parameters. On the contrary, the site amplification is less
553 pronounced and independent from the proposed site parameters, for vibration periods of the
554 FF motion higher than 1 s.
555 Nonlinear effects are negligible for small earthquakes and for vibration periods of strong
556 ground motions longer than 1 s. Whereas, they are significant for short- and middle-periods of
557 strong earthquakes. In particular, soil profiles having dominant period $T_0$ higher than that of
558 the homogeneous profile exhibit significant nonlinear effects. In addition, soil profiles with
559 negative value of $B_{30}$ (i.e. velocity inversion) and profiles with high value of $B_{30}$ lead to
560 pronounced nonlinear site effects.
561 Average amplification factors are compared to those suggested by Eurocode 8 [25] and New
562 Zealand Standard [26] building codes, and by Pitilakis et al. [18]. The obtained results
563 demonstrate that the ground type classification proposed by Eurocode 8 [25], based on $v_{s,30}$
564 only, is not suitable. The comparison to the amplification factors proposed by Pitilakis et al.
565 [18] shows that the introduction of complementary site proxies makes the ground type
566 classification more adequate. In fact, the computed average spectral amplification factors *SA*
567 are comparable to those estimated by Pitilakis et al. [18].
568 The average amplification factors computed for soil profiles with a velocity inversion are
569 lower than for the profiles having monotonic shear wave velocity profiles.
570 This research confirms that it is possible to improve the current ground type classification

taking into account simple and accessible site parameters complementary to $v_{s,30}$. Accounting for complementary site proxies in the ground type classification, such as the dominant frequency of the site $f_0$ and the shear wave velocity gradient $B_{30}$, allow a better prediction of the expected amplification, in particular for short vibration periods of the FF motion, up to 1s. Further work should be done to analyze the results for soil profiles having different ground types according to the Eurocode 8 (only ground type C has been discussed in this research) and depth $H_{800}$.

## 6. References


[1] Semblat JF, Kham A, Parara E, Bard P, Pitilakis K, Makra K, et al. Seismic wave amplification : Basin geometry vs soil layering . Soil Dynamics and Earthquake Eng. 2005; 25(7-10):529-538. 2009.

[2] Borcherdt RD. Estimates of site-dependent response spectra for design (methodology and justification). Earthq Spectra 1994;10:617–53.

[3] Dickenson, S. E. and RBS. Nonlinear dynamic response of soft and deep cohesive soil deposits. Proc. Int. Work. site response Subj. to strong Earthq. motions, 1996, p. 67–81.

[4] Dobry, R., Borcherdt, R. D., Crouse, C. B., Idriss, I. M., Joyner, W. B., Martin, G. R., Seed RB. New site coefficients and site classification system used in recent building seismic code provisions. Earthq Spectra 2000;16:41–67.

[5] Seyhan, E., Stewart, J. P., Ancheta, T. D., Darragh, R. B., & Graves RW. NGA-West2 site database. Earthq Spectra 2014;30:1007–24. doi:10.1193/062913EQS180M.

[6] Seyhan E, Stewart JP. Semi-Empirical Nonlinear Site Amplification from NGA-West2 Data and Simulations. Earthq Spectra 2014;30:1241–56. doi:10.1193/063013EQS181M.

[7] Derras B, Bard PY, Cotton F. Site-condition proxies, ground motion variability, and data-driven GMPEs: Insights from the NGA-West2 and RESORCE data sets. Earthq Spectra 2016;32:2027–56. doi:10.1193/060215EQS082M.

[8] Park D, Hashash YMA. Probabilistic seismic hazard analysis with non linear site effects in the Mississippi embayment. 13 th World Conf. Earthq. Eng., 2004, p. 1549.

[9] Mucciarelli M, Gallipoli MR. Comparison between Vs30 and other estimates of site amplification in Italy. First Eur Conf Earthq Eng Seismol 2006:270.

[10] Castellaro S, Mulargia F, Rossi PL. Vs30: Proxy for Seismic Amplification? Seismol Res Lett 2008;79:540–3. doi:10.1785/gssrl.79.4.540.

[11] Cadet H, Bard PY, Duval AM. a New Proposal for Site Classification Based on Ambient Vibration Measurements and the Kiknet Strong Motion Data Set. 14th World Conf Earthq Eng 2008.

[12] Luzi L, Puglia R, Pacor F, Gallipoli MR, Bindi D, Mucciarelli M. Proposal for a soil classification based on parameters alternative or complementary to Vs,30. Bull Earthq Eng 2011;9:1877–98. doi:10.1007/s10518-011-9274-2.

[13] Cadet H, Bard PY, Duval AM, Bertrand E. Site effect assessment using KiK-net data: Part 2-site amplification prediction equation based on f0 and Vsz. Bull Earthq Eng 2012;10:451–89. doi:10.1007/s10518-011-9298-7.

[14] Derras B, Bard PY, Cotton F. VS30, slope, H800 and f0: Performance of various site-condition proxies in reducing ground-motion aleatory variability and predicting nonlinear site response 4. Seismology. Earth, Planets Sp 2017;69:0–21. doi:10.1186/s40623-017-0718-z.

[15] Castelli F, Cavallaro A, Grasso S, Lentini V. Seismic microzoning from synthetic ground motion earthquake scenarios parameters: The case study of the city of Catania (Italy). Soil Dyn Earthq Eng 2016;88:307–27. doi:10.1016/j.soildyn.2016.07.010.

[16] Steidl JH. Site response in southern California for probabilistic seismic hazard analysis. Bull Seismol Soc Am 2000;90:149–69. doi:10.1785/0120000504.

[17] Kotha, S. R., Cotton, F., & Bindi D. A New Approach to Site Classification : Mixed-effects Ground Motion Prediction Equation with Spectral Clustering of Site Amplification Functions. Soil Dyn Earthq Eng 2018;110:318–29.

[18] Pitilakis K, Riga E, Anastasiadis A. New code site classification, amplification factors and normalized response spectra based on a worldwide ground-motion database. Bull Earthq Eng 2013;11:925–66. doi:10.1007/s10518-013-9429-4.

[19] Castellaro S, Mulargia F. Simplified seismic soil classification: The Vfz matrix. Bull Earthq Eng 2014;12:735–54. doi:10.1007/s10518-013-9543-3.

[20] Zhao JX, Irikura K, Zhang J, Fukushima Y, Somerville PG, Asano A, et al. An empirical site-classification method for strong-motion stations in Japan using H/V response spectral ratio. Bull Seismol Soc Am 2006;96:914–25. doi:10.1785/0120050124.

[21] Gallipoli MR, Mucciarelli M. Comparison of site classification from VS30, VS10, and HVSR in Italy. Bull Seismol Soc Am 2009;99:340–51. doi:10.1785/0120080083.

[22] Boudghene Stambouli A, Zendagui D, Bard PY, Derras B. Deriving amplification factors from simple site parameters using generalized regression neural networks: Implications for relevant site proxies. Earth, Planets Sp 2017;69. doi:10.1186/s40623-017-0686-3.

[23] Zhu C, Pilz M, Cotton F. Which is a better proxy, site period or depth to bedrock, in modelling linear site response in addition to the average shear-wave velocity? Bull Earthq Eng 2019:1–24. doi:10.1007/s10518-019-00738-6.

[24] Ciancimino A, Foti S, Lanzo G. Stochastic analysis of seismic ground response for site classification methods verification. Soil Dyn Earthq Eng 2018;111:169–83.

doi:10.1016/j.soildyn.2018.04.006.

[25] European Committee for Standardization (CEN). Eurocode 8: Design of structures for earthquake resistance—Part 1: General rules, seismic actions and rules for buildings (EN 1998-1: 2004). Eur Comm Norm Brussels 2004.

[26] 1170.5:2004 NZS. Structural Design Actions - Part 5: Earthquake actions- New Zealand. Struct Des Actions 2004.

[27] Brûlé S, Javelaud E. H/V method in geotechnical engineering. Application to a two layers model. Rev Fr Geotech 2013;142.

[28] Régnier J, Cadet H, Bonilla LF, Bertrand E, Semblat JF. Assessing Nonlinear Behavior of Soils in Seismic Site Response : Statistical Analysis on KiK-net Strong-Motion Data. Bull Seismol Soc Am 2013;103:1750–70. doi:10.1785/0120120240.

[29] Régnier J, Cadet H, Bard PY. Empirical quantification of the impact of nonlinear soil behavior on site response. Bull Seismol Soc Am 2016;106:1710–9. doi:10.1785/0120150199.

[30] Santisi d'Avila MP, Lenti L, Semblat JF. Modelling strong seismic ground motion: Three-dimensional loading path versus wavefield polarization. Geophys J Int 2012;190:1607–24. doi:10.1111/j.1365-246X.2012.05599.x.

[31] Santisi d'Avila MP, Semblat JF, Lenti L. Strong ground motion in the 2011 Tohoku earthquake: A one-directional three-component modeling. Bull Seismol Soc Am 2013;103:1394–410. doi:10.1785/0120120208.

[32] Yokota K, Imai T, Konno M. Dynamic deformation characterisitcs of soils 1981:13–37.

[33] Darendeli MB. Development of a new family of normalized modulus reduction and material damping curves. PhD thesis, The University of Texas at Austin, 2001.

[34] Massa M, Pacor F, Luzi L, Bindi D, Milana G, Sabetta F, et al. The ITalian

ACcelerometric Archive (ITACA): Processing of strong-motion data. Bull Earthq Eng 2010. doi:10.1007/s10518-009-9152-3.

[35] Ambraseys NN, Smit P, Douglas J, Margaris B, Sigbjörnsson R, Ólafsson S, et al. Internet site for European strong-motion data. Boll Di Geofis Teor Ed Appl 2004;45:113–29.

[36] PEER PEERC. PEER Ground Motion Database. Shallow Crustal Earthquakes Act Tecton Regimes, NGA-West2 2013.

[37] Cameron WI, Green RA. Soil Nonlinearity versus Frequency Effects. Int Work Uncertainties Nonlinear Soil Prop Their Impact Model Dyn Response 2004:1–7.

[38] Newmark NM, Hall WJ. Earthquake Spectra and Design, Earthquake Engineering Research Center. Berkeley,CA 1982:103.

[39] Kawase H. Strong motion characteristics and their damage impact to structures during the off pacific coast of tohoku earthquake of march 11, 2011: How extraordinary was this M 9. 0 earthquake. 4th IASPEI/IAEE Int. Symp., 2011.

[40] Régnier J, Bonilla LF, Bard PY, Bertrand E, Hollender F, Kawase H, et al. International benchmark on numerical simulations for 1D, nonlinear site response (Prenolin): Verification phase based on canonical cases. Bull Seismol Soc Am 2016;106:2112–35. doi:10.1785/0120150284.

[41] Régnier J, Bonilla LF, Bard PY, Bertrand E, Hollender F, Kawase H, et al. Prenolin: International benchmark on 1D nonlinear: Site-response analysis—validation phase exercise. Bull Seismol Soc Am 2018;108. doi:10.1785/0120170210.

[42] Joyner WB, Chen ATF. Calculation of nonlinear ground response in earthquakes. Bull Seismol Soc Am 1975;65:1315–36.

[43] Iwan W.D. On a class of models for the yielding behavior of continuous and composite systems. J Appl Mech 1967;34:612–7.

[44] Joyner WB. A method for calculating nonlinear seismic response in two dimensions. Bull Seismol Soc Am 1975;65:1337–57.

[45] Régnier J, Bonilla LF, Bertrand E, Semblat JF. Influence of the VS profiles beyond 30 m depth on linear site effects: Assessment from the KiK-net Data. Bull Seismol Soc Am 2014;104:2337–48. doi:10.1785/0120140018.

[46] Rey J, Faccioli E, Bommer JJ. Derivation of design soil coefficients (S) and response spectral shapes for Eurocode 8 using the European Strong-Motion Database. J Seismol 2002;6:547–55. doi:10.1023/A:1021169715992.

[47] Housner GW. Spectrum Intensities of Strong-Motion Earthquakes. Symp Earthq Blast Eff Struct 1952:20–36.

[48] Kramer S. Geotechnical Earthquake Engineering. Prentice H. Upper Saddle River: 1996.